University of Huddersfield Repository

Tran, Van Tung, Al Thobiani, Faisal and Ball, Andrew

An Application to Transient Current Signal based Induction Motor Fault Diagnosis of Fourier-Bessel Expansion and Simplified Fuzzy ARTMAP

Original Citation

Tran, Van Tung, Al Thobiani, Faisal and Ball, Andrew (2013) An Application to Transient Current Signal based Induction Motor Fault Diagnosis of Fourier-Bessel Expansion and Simplified Fuzzy ARTMAP. Expert Systems With Applications, 40 (13). pp. 5372-5384. ISSN 0957-4174

This version is available at http://eprints.hud.ac.uk/17172/

An Application to Transient Current Signal based Induction Motor Fault Diagnosis of Fourier-Bessel Expansion and Simplified Fuzzy ARTMAP

Van Tung Tran [a,*], Faisal AlThobiani [a], Andrew Ball [a], Byeong-Keun Choi [b]

[a] *School of Computing and Engineering, University of Huddersfield, Queensgate, Huddersfield HD1 3DH, UK*

[b] *Department of Energy and Mechanical Engineering, Gyeongsang National University, Institute of Marine Industry, 445 Inpyeong-dong, Tongyeong 650-160, South Korea*

ABSTRACT

The start-up transient signals have been widely used for fault diagnosis of induction motor because they can reveal early defects in the development process, which are not easily detected with the signals in the steady state operation. However, transient signals are non-linear and contain multi components which need a suitable technique to process and identify the fault pattern. In this paper, the fault diagnosis problem of induction motor is conducted by a data driven framework where the Fourier-Bessel (FB) expansion is used as a tool to decompose transient current signal into series of single components. For each component, the statistical features in the time and the frequency domains are extracted to represent the characteristics of motor condition. The high dimensionality of the feature set is solved by generalized discriminant analysis (GDA) implementation to decrease the computational complexity of classification. In the meantime, with the aid of GDA, the separation of the feature clusters is increased, which enables the more classification accuracy to be achieved. Finally, the reduced dimensional features are used for classifier to perform the fault diagnosis results. The classifier used in this framework is the simplified fuzzy ARTMAP (SFAM) which belongs to a special class of neural networks (NNs) and provides a lower training time in comparison to other traditional NNs. The proposed framework is validated with transient current signals from an induction motor under different conditions including bowed rotor, broken rotor bar, eccentricity, faulty bearing, mass unbalance and phase unbalance. Additionally, this paper provides the comparative performance of (i) SFAM and support vector machine (SVM), (ii) SVM in the framework and SVM combined with wavelet transform in previous studies, (iii) the use of FB decomposition and Hilbert transform decomposition. The results show that the proposed diagnosis framework is capable of significantly improving the classification accuracy.

Keywords: Fault diagnosis; Transient current signal; Induction motor; Fourier-Bessel expansion; Simplified fuzzy ARTMAP.

1. Introduction

Induction motors are one of the most widely used electrical machines in industry due to their ruggedness and versatility. However, they are susceptible to many types of fault sourced from mechanical and electrical stresses which permanently exist in motor's operation. The mechanical stresses caused by overloads and abrupt load changes can lead to bearing faults and rotor bar breakage. Meanwhile, the electrical stresses may produce stator winding short circuits and cause a complete motor failure. According to motor reliability studies (Bonnett, 1992), the faults in induction motor are typically related to bearings, stator, rotor, and the remainder that are a consequence of a great variety of other faults. These faults are often sources of increasing the maintenance costs, disturbances in production activity, and the main reason for stoppage of operation. Therefore, reliable diagnostic methodologies are of necessity to enable effective maintenance and operational costs.

In order to detect and identify these faults, several approaches using combinations of mechanical and electrical monitoring have been used. Among these, electrical monitoring with emphasis on inspecting the stator current has gradually become one of the most important approaches and received special interest from researchers. The widely used scheme in this area is motor current signature analysis (MCSA). Many studies have been developed based on MCSA under steady state operating conditions (Elkasabgy et al., 1992; Kliman et al., 1988; Schoen et al., 1995a; Schoen et al., 1995b; Nandi et al., 1998; Thomson & Fenger, 2001; Benbouzid, 2000). However, MCSA depends not only on the accuracy of measurements, but also on the ability to differentiate between normal and faulty conditions (Henry et al., 2002). Furthermore, the techniques using steady state conditions are effectively used only when the machines are almost fully loaded and running at a constant speed. Conversely, they result in less accuracy when applied to machines that are lightly loaded or operated predominantly under transient conditions (Douglas & Pillay, 2005). For example, if the load torque varies with rotational speeds, then the motor current spectral harmonics produced by the load overlap the harmonics caused by broken bars, making the fault detection task difficult.

Researches on transient signals of induction motors have been attracted attention in recent times due to the fact that the machine is subjected to stresses above normal condition during the start-up. These stresses could highlight machine defects that are early in their development and not easily detected at steady state conditions (Niu et al., 2008). However, transient signals are usually non-linear, non-stationary, and contain several components with different amplitudes and frequencies. These lead to difficulty in using common methods such as fast Fourier transform (FFT) to analyze the fault symptom and diagnose the faults in the induction motor. Owing to limitations of the FFT which only provides the spectral content of the signal but gives no information regarding where in time those spectral components appear (Ramesh Babu et al., 2008), other techniques were proposed to deal with non-stationary signal such as short-time

Fourier transform (STFT) and Hilbert-Huang transform (HHT). However, STFT also has limitation which is its fixed time-frequency resolution whilst the limitations of HHT were reported in (Peng et al., 2005; Qin et al., 2006; Rato et al., 2008). Another outstanding technique implemented for transient current signals is the wavelet transform. Niu et al. (Niu et al., 2008) applied a smoothing technique to the motor transient current signal and subtracted the smoothed signal from the original one to obtain the residual. Then, a discrete wavelet transforms (DWT) and decision-level fusion model were implemented to decompose the residual into different details and classify the faults based on these decomposed details, respectively. Similarly, Widodo et al. (Widodo et al., 2009) combined DWT for signal decomposition, independent component analysis (ICA) and principle component analysis (PCA) for feature extraction, and support vector machine (SVM) for classification to diagnose the faults of induction motors using the transient signal. Other studies used wavelet transforms and transient current signal for fault diagnosis could be found in (Widodo & Yang, 2008; Cabal-Yepez et al., 2012; Ebrahimi et al., 2012). Obviously, smoothing the original transient signal could eliminate the valuable information which leads to a reduction in the diagnosis accuracy. Furthermore, the wavelet transform has a drawback where the basis function has to be defined a priori and this choice may influence the final results.

Recently, Fourier-Bessel (FB) expansion has been introduced as a suitable technique for non-stationary signal analysis because of that it has unique coefficients for a given signal and the Bessel functions are aperiodic and decay over time (Pachori & Sircar, 2008). FB expansion has been widely used for performing speech-related applications such as speech enhancement, speaker identification, speech recognition and synthesis, etc. (Schroeder, 1993; Gopalan, 2001; Gopalan et al., 1997; Chen & Gurgen, 1990). In the fault diagnosis area, FB expansion in association with the Wigner-Ville distribution has been used for gear fault study (D'Elia et al., 2012).

In this paper, a new framework of data driven approach as shown in Fig. 1 is proposed for fault diagnosis of induction motor. This framework involves three stages which are signal decomposition, feature representation and reduction, and fault diagnosis. The FB expansion is introduced to the framework in the first stage to decompose the transient current signals acquired from different induction motor conditions into the FB series. Each single component in the signal is isolated by a non-overlapping cluster of FB coefficients. By using FB decomposition, the shortcoming of wavelet transform and the removal of useful information due to smoothing and subtracting are eliminated. In the meanwhile, the component which can characterize the difference among motor conditions is selected in this stage. In the second stage, statistical features in the time domain and the frequency domain are extracted for each single component. Normally, these features can cure problems of dimensionality and peaking phenomenon that greatly degrade the classification accuracy. Therefore, the dimensionality

reduction is necessarily performed to reduce the dimension of a feature set. In fault diagnosis, there have been numerous approaches for feature reduction such as ICA, PCA, and genetic algorithms, etc. In this study, the generalized discriminant analysis (GDA) (Baudat & Anouar, 2000) based feature reduction is investigated with the aim of improving the classification performance. In the last stage, the reduced dimensional feature set is split into training set and test set to build the classifier and validate it, respectively. The classifier used herein is simplified fuzzy ARTMAP (SFAM) (Kasuba, 1993) which was derived from the fuzzy ARTMAP (Carpenter et al., 1992) network. SFAM provides a lower training time and higher recognition accuracy in comparison to other traditional neural networks (Palaniappan & Eswaran, 2009; Jervis et al., 1999); therefore, it has been applied in numerous classification problems (Palaniappan & Eswaran, 2009; Rajasekaran & Pai, 2000a; Rajasekaran & Pai, 2000b; Vuskovic & Du, 2002).

Fig. 1 The proposed framework for fault diagnosis

In order to appraise the effect of the proposed framework, three comparative studies of classification accuracy are conducted in this paper: (i) the use SFAM and SVM as classifiers in the framework, (ii) SVM in this framework and SVM combined with DWT in previous works, (iii) the use of FB decomposition and another decomposition method which was derived from Hilbert transform and called Hilbert vibration decomposition (HVD) (Feldman, 2006; Feldman, 2011). Theoretically, HVD primarily estimates the global instantaneous frequency (IF) via low-pass filtering; then the corresponding envelope is calculated on the basis of the global IF via synchronous detection. As a result, HVD is able to decompose both wideband and narrowband signals and is suitable for multicomponent non-stationary signals or motion of non-linear dynamic system (Feldman, 2008). A comparison of HVD and the well-known empirical mode decomposition method (Huang et al., 1998) could be found in (Feldman, 2008) for interested readers who need more explanation.

2. Background knowledge

2.1. Fourier-Bessel (FB) expansion

Let $x(t)$ be a discrete-time signal considered over an arbitrary interval $(0, a)$, the zero-order FB expansion is expressed as

$$x(t) = \sum_{m=1}^{M} C_m J_0(\lambda_m t/a) \tag{1}$$

where $J_0(\cdot)$ are the zero-order Bessel functions (Schroeder, 1993), which are the solution of the Bessel's differential equation. The FB coefficients C_m are computed via the relation

$$C_m = \frac{2\int_0^a tx(t)J_0(\lambda_m t/a)dt}{a^2[J_1(\lambda_m)]^2} \tag{2}$$

where $J_1(\cdot)$ are the first-order Bessel functions, λ_m, $m = 1,...,M$,are the ascending order positive roots of $J_0(t) = 0$.

The order and range of non-zero coefficients of the FB expansion of the signal are changed as the center frequency and the bandwidth of the signal are varied. There is a one-to-one correspondence between the frequency content of the signal and the order m where the coefficient attains peak magnitude (Pachori & Sircar, 2008). Note that the FB series coefficients C_m are unique for a given signal $x(t)$, similar to the Fourier coefficients. The integral in the numerator of Eq. (2) is the finite Hankel transform (FHT). Many numerical computation methods have been proposed for calculating the FHT and the corresponding FB coefficients in (Oppenheim et al., 1978; Cavanagh & Cook, 1979; Candel, 1981a; Candel, 1981b; Oppenheim et al., 1980). In this paper, the FHT and the corresponding FB coefficients are calculated by using numerical method proposed in (Guizar-Sicairos & Gutierrez-Vega, 2004) due to fast computation.

Since the Fourier transform of the Bessel function

$$s(t) = J_0(\lambda_m t/a) \tag{3}$$

is given by

$$S(\omega) = \frac{1}{\sqrt{(\lambda_m/a)^2 - \omega^2}} \quad \text{for} |\omega| < \lambda_m/a \tag{4}$$

in the spectral domain, each term $C_m J_0(\lambda_m t/a)$ of Eq. (1) has an approximate bandwidth $\omega_B \cong \lambda_m/a$. Therefore, the reconstruction of $x(t)$ using the first M terms has a maximum band width of $\omega_{\max} \cong \lambda_m/a$ (Arfken, 1996; Pachori & Sircar, 2007).

For multi-component signal, i.e. a signal $x(t)$ that is the sum of N signal $x_i(t)$, where $x_i(t)$ can be expanded in FB series via Eq. (1). A multi-component signal can be written as:

$$x(t) = \sum_{i=1}^{N} x_i(t) = \sum_{i=1}^{N}\sum_{m=1}^{M} C_{m_i} J_0(\lambda_m t/a) = \sum_{m=1}^{M}\left(\sum_{i=1}^{N} C_{m_i}\right) J_0(\lambda_m t/a) \tag{5}$$

By interchanging the summations, the FB series coefficients of a multicomponent signal can be obtained as:

$$C_m = \sum_{i=1}^{N} C_{m_i} \tag{6}$$

Eq. (6) implies that the resulting set of coefficients $\{C_m\}$ is obtained by summing the coefficients $\{C_{m_i}\}$ of the component signals. If the components of the composite signal are well separated in the frequency domain, then the signal components will be associated with various distinct clusters of non-overlapping FB coefficients. Therefore, each component of the

signal can be generated separately by identifying and separating the corresponding FB coefficients.

2.2. Generalized discriminant analysis

The generalized discriminant analysis (GDA) (Baudat & Anouar, 2000; Kim & Kittler, 2005) deals with a nonlinear classification using a kernel function Φ which maps the original space **X** into a new high-dimensional features space **Z**. The within-class scatter and between-class scatter matrix of the nonlinearly mapped data is

$$B^{\phi} = \sum_{c=1}^{C} M_c m_c^{\phi} (m_c^{\phi})^T, \quad W^{\phi} = \sum_{c=1}^{C} \sum_{x \in X_c} \phi(x)\phi(x)^T \tag{7}$$

where m_c^{ϕ} is the mean of class X_c and Z, M_c is the number of samples belonging to X_c. The aim of the GDA is to find such projection matrix U^{ϕ} that maximizes the ratio

$$U_{opt}^{\phi} = \arg\max_{U^{\phi}} \frac{|(U^{\phi})^T B^{\phi} U^{\phi}|}{|(U^{\phi})^T W^{\phi} U^{\phi}|} = [u_1^{\phi}, u_2^{\phi}, ..., u_N^{\phi}] \tag{8}$$

The vectors u^{ϕ} can be found as the solution of the generalized eigenvalue problem i.e., $B^{\phi} u_i^{\phi} = \lambda_i W^{\phi} u_i^{\phi}$. The training vectors are supposed to be centered (zero mean, unit variance) in the feature space **Z**. From the theory of reproducing kernels, any solution $u^{\phi} \in Z$ must lie in the span of all training samples, i.e.

$$u^{\phi} = \sum_{c=1}^{C} \sum_{i=1}^{M_c} \alpha_{ci} \phi(x_{ci}) \tag{9}$$

where α_{ci} are some real weights and x_{ci} is the ith sample of the class c. The solution is obtained by solving

$$\lambda = \frac{\alpha^T KDK\alpha}{\alpha^T KK\alpha} \tag{10}$$

where $\alpha = (\alpha_c)$, $c = 1,...,C$ is a vector of weights with $\alpha_c = (\alpha_{ci})$, $i = 1,...,M_c$. The kernel matrix $K(M \times M)$ is composed of the dot products of nonlinearly mapped data, i.e.

$$K = (K_{kl}); \quad k = 1,...,C; l = 1,...,C \tag{11}$$

where $K_{kl} = (k(x_{ki}, x_{lj}))$; $i = 1,...,M_k$; $j = 1,...,M_l$. The matrix $D(M \times M)$ is a block diagonal matrix such that

$$D = (D_c); \quad c = 1,...,C \tag{12}$$

where the cth on the diagonal has all elements equal to $1/M_c$. Solving the eigenvalue problem yields the coefficient vector α that defines the projection vectors $u^{\phi} \in Z$. A projection of a testing vector x_{test} is computed as

$$(u^{\phi})^T \phi(x_{test}) = \sum_{c=1}^{C} \sum_{i=1}^{M_c} \alpha_{ci} k(x_{ci}, x_{test}) \tag{13}$$

The procedure of the proposed algorithm could be summarized as follows:

(i) Compute the matrices K and D by solving the Eq. (11) and Eq. (12).

(ii) Decompose K using eigenvector decomposition

(iii) Compute eigenvectors α and eigenvalues of Eq. (8)

(iv) Compute u^ϕ using α_{ci} from Eq. (9) and normalize them

(v) Compute projections of the test points onto the eigenvectors u^ϕ using Eq. (13)

2.3. Simplified fuzzy ARTMAP network

The architecture of simplified fuzzy ARTMAP (SFAM) is show in Fig. 2 (Rajasekaran & Pai, 2000a; Rajasekaran & Pai, 2000b). The input into the network flows through the complement coder where it is normalized to a range from 0 to 1 and stretched to double size by providing the fuzzy compliment. This expanded input is then passed to the input layer. Each node in the output category layer is linked through a set of top-down weights to each node in the input layer. The N nodes in category layer hold the names of the M categories or classes that the SFAM has to learn to recognize. When active during testing, an output category node indicates the class by pointing to the corresponding category classification node. The vigilance parameter (VP) ρ, which ranges from 0 to 1, has to be chosen to determine the number of classes found. Match tracking portion of the network lets itself adjust ρ if classification errors are found during training.

Fig. 2 The architecture of SFAM network

The training procedure is described as follows. For a given input vector a of d features, the complement coded vector a' represents the absence of each feature, where a' is defined as

$$a' = 1 - a \tag{14}$$

The complement coded input vector I internal to SFAM is given by two-dimensional vector:

$$I = (a, a') = (a_1, a_2, ..., a_d, a'_1, a'_2, ..., a'_d) \tag{15}$$

The normalization of input vector is expressed as

$$|I| = |(a, a')| = \sum_{i=1}^{d} a_i + (d - \sum_{i=1}^{d} a_i) \tag{16}$$

where the norm $| \cdot |$ is defined as $|p| = \sum_{i=1}^{d} p_i$

When SFAM is presented an input pattern whose complement coded representation is I, all output nodes become active to some degree. This output activation is denoted by T_j for the jth output node:

$$T_j(I) = \frac{|I \wedge w_j|}{\alpha + |w_j|} \tag{17}$$

8

where α is kept as a small value close to 0 usually about 0.001 (Carpenter et al., 1992), $\wedge$ is the fuzzy AND operator defined by $(a \wedge b)_i = \min(a_i, b_i)$ where a and b are fuzzy vector, w_j is the corresponding weight vector which the initial condition is $w_{j1}(0) = ... = w_{j,2d}(0) = 1$. The winning output node is the node with the highest activation function T_j. If more than T_j is maximal, the output node j with the smallest index is arbitrarily chosen to break the tie. The category associated with the winning output node is described as the network's classification of the current input pattern.

The degree of match between the output category node and an input vector is given by the match function (MF) defined as

$$MF(I, w_j) = \frac{|I \wedge w_j|}{|I|} \tag{18}$$

When used in conjunction with VP, MF value states whether the current input is a good enough match to a particular output node to be encoded by that output node, or instead, whether a new output node should be formed to encode the input pattern. If MF value is greater than the VP, the network is said to be in a state of resonance. Resonance means that output node j is good enough to encode the input I, provided that output node j represents the same category as input I. A network state called "mismatch reset" occurs if MF is less than VP. This state indicates that the current output node does not meet the encoding granularity represented by VP and therefore cannot update its weights even if the input patterns' category is equal to the category of the winning output node.

Once a winning output node j has been selected to learn a particular input pattern I, the top-down weight vector w_j from the output node is updated according to the equation:

$$w_j^{new} = \beta(I \wedge w_j^{old}) + (1 - \beta)w_j^{old} \tag{19}$$

where β $(0 \le \beta \le 1)$ is the learning rate. Once SFAM has been trained, the equivalent of a "feed forward" pass for an unknown pattern classification consists of passing the input pattern through the complement coder and into the input layer. The output node activation function is evaluated and the winner is the one with the highest value. The category of the input pattern is the one with which the winning output node is associated.

3. Application of the proposed framework and discussion

3.1. Experiment and data acquisition

To validate the proposed framework, an experiment was carried out using a test-rig which consists of a motor, pulleys, belt, shaft, and fan with changeable blade pitch angle that represents the load, as shown in Fig. 3. The load can be changed by adjusting the blade pitch angle or the number of blades. Seven three-phase induction motors of 0.5 kW, 60 Hz, 4-pole

were used to generate data. One of these motors is in normal condition (NOR) whilst the others are faulty motors involving bowed rotor (BR), broken rotor bar (BRB), eccentricity (ECC), faulty bearing (outer race) (FBO), mass unbalance (MUN), and phase unbalance (PUN). The conditions of these motors are described in Table 1. For acquiring data from test rig, three AC current probes were used to measure the transient stator current of the three-phase power supply. The data sample was 16,384 measurements under a fixed load condition. For each condition, 20 samples were taken.

Fig. 3 Test rig for experiment

Table 1 The description of motor conditions

3.2. FB expansion based signal decomposition

Due to the existence of the line frequency, the current signals obtained from different motor conditions are similar. For instance, the similarity of NOR, BR, ECC, and MUN conditions is shown in Fig. 4. This similarity leads to increasing difficulty in recognizing the fault patterns. To solve this issue, some previous works (Niu et al., 2008; Widodo et al., 2009) used smoothing in association with subtracting techniques to reduce/remove the line frequency. However, smoothing the signal could also eliminate useful information which reduces classification accuracy. In this paper, FB decomposition is directly applied to transient current signals to separate them into single component signals so that elimination of useful information is avoided.

Fig. 4 The similarity of transient current signals

Fig. 5 correspondingly shows the original transient current signal in phase A of the BR fault, its spectrum, and its FB coefficients. It can be seen in Fig. 5(c) that there are three abrupt changes and a distinct cluster of non-overlapping FB coefficients approximately located at the order 380, 1150, and 1900 respectively. These indicate that the original signal is constituted from three single components. By choosing proper coefficient bands and substituting to Eq. (1), the single components are obtained as shown in Fig. 6. As observed, the first and the last components are identical in shape with the original signal, especially the first component which has nearly same the amplitude, while the second component is significantly different. The reason for these phenomena is that the single components depend on the values of the FB coefficients. As shown in Fig. 5(c), the abrupt changes of FB coefficients for the first component are high while those of the remainders are very low. Fig. 7 shows a comparison of the original bowed rotor signal, the reconstructed signal from the three components and the residual. As observed from this figure, the original signal could be reconstructed with a high degree of accuracy in shape and amplitude from its single components. However, the residual is

still large enough to contain useful information for fault diagnosis; therefore, this residual is used as the last component of the decomposition process for fault diagnosis.

Fig. 5 a) Transient current signal of the bowed rotor in phase A, b) Current spectrum, c) FB coefficients
Fig. 6 Single components of the bowed rotor signal in phase A
Fig. 7 The bowed rotor signal in phase A: a) Original, b) Reconstructed, c) Residual

Similarly, the process of identifying the components based on FB coefficients is repeated for the remaining phases (B and C) as well as all the remaining conditions. In total, 1680 (3×4×140) components are obtained and used for the next stage. Fig. 8 shows the obtained components of all motor conditions in phase A. As observed in Figs. 8(a) and 8(b) which respectively present the first and the second components, the differences between each component are not clearly identified except the components of the bowed rotor. The most obvious difference among these conditions could be recognized as the differences in the time durations reaching to the steady state. However, it is easy to distinguish the differences from the conditions of the third and the fourth components, as shown in Figs. 8(c) and (d). The differences observed from these figures are not only the duration reaching steady state but also the amplitude variations of the motor conditions. Therefore, the component 3 and 4 are chosen as the signals inputted into the next stages of diagnosis framework.

Fig. 8 The components of the motor conditions: a) Component 1, b) Component 2, c) Component 3, and d) Residual

3.3. Feature extraction and reduction

Normally, raw signals are rarely usable in their forms due to the redundancy and huge dimensionality which leads to difficulties of storage and inaccuracy in analysis. Thus, feature extraction is an essential signal preprocessing technique and plays a crucial role in fault diagnosis problem. Extracting features from raw signal is a process of drawing the useful information to remove artifacts and reduce the dimensionality. However, this process must preserve as much as possible the characteristics which indicate the fault pattern. In this study, feature extraction using statistical feature parameters from the time domain and the frequency domain is utilized for the chosen components of the previous stage. For each component, sixty-three features consisting of ten features in the time domain, three features in the frequency domain, and eight features of regression estimation are extracted from the three current phases. The descriptions of these features are as shown from Table 2 to Table 4.

Table 2 The statistical features in the time domain
Table 3 The statistical features in the frequency domain
Table 4 The statistical features of regression estimation

In order to observe the feature distribution of each single component, three features can be arbitrarily selected from the feature set. This visualization only provides the information to understand how the features distribute in same machine condition and how the clusters of the features separate in the different conditions. From this visualization, the reason of misclassification, if any, can be estimated based on the overlap of the features. Fig. 9 shows the distribution of the three-first features involving mean, RMS, and SF of the components 3 and 4. It can be seen that only the features of BR are slightly well clustered in the component 3, as depicted in Fig. 9(a), the remaining features are disorder and overlap with each other which significantly makes difficulty in classification.

Fig. 9 The structure of the three-first features: a) Component 3, b) Component 4 (residual)

To increase the separation among the feature clusters and reduce the feature dimensionality for effective computation, GDA is continuously applied to the original feature set of each component. Theoretically, GDA attempts to maximize the Fisher criterion in the high-dimensional space that is constructed using the kernel function. In this way, GDA allows for the construction of nonlinear mappings that maximize the class separability in the data. The sufficient amount of necessary features to characterize the machine condition can be gained based on the eigenvalue of the covariance matrix (Yang & Widodo, 2009). As a result shown in Fig. 10, sixty-three features in the feature space are reduced to fifteen where the non-zero eigenvalues of covariance matrix are retained in the GDA space. The other features are discarded due to their very small eigenvalue. Furthermore, the structures of patterns related to the different conditions are reconstructed as shown in Fig. 11. It can be seen that the features of the same condition in new space are located close to each other and are well separated from the other conditions. This makes the classification process easier and more accurate. Thus, the new reduced feature set not only increases the classification performance but also provides an appropriate tool for a better discrimination of different motor conditions. As observed in Fig. 11, although the disorder of features is eliminated and the cluster is well carried out, overlap still exists in some group features, which can cause the inaccuracy in the diagnosis process. In Fig. 11(a), BR, BRB, and PUN are well clustered; the remaining features of the component 3 are still overlapped. The same problem occurs in the features of the component 4, as illustrated in Fig. 11(b). However, the separation is better than that of the component 3, in which the overlap happens only between the features of ECC and PUN while the others are well discriminated.

Fig. 10 Eigenvalue of covariance matrix for feature reduction
Fig. 11 The feature structure in the GDA space: a) Component 3, b) Component 4

3.4. Classification results of SFAM and the comparative studies

The data sets of the features from previous stage have 140 samples obtained for 7 conditions for each component. This set is randomly partitioned by holdout validation method into a training set with 10 samples for each condition and a test set with the remaining samples. In the training mode, SFAM is trained by basic network setting, i. e. fast learning $\beta = 1$ and conservative mode $\alpha = 0.001$. The value of VP varies from 0 to 0.9 with an increment step of 0.1 to investigate the performance. The accuracy of classification in this mode achieves 100% for all values of VP. In the testing mode, the classifier is applied to the test data to validate the accuracy of the diagnosis, where the classification results are presented in Fig. 12. It can be seen that, the accuracy for the chosen component signals (the component 3 and 4) is very high, which the average values are respectively of 99.14% and 100%. Obviously, the residual gives a better result than that of the other component. The reason is that the components obtained from the decomposition process have eliminated the similarity caused by the line frequency in the transient signal; hence, the residual can retain useful information characterizing the difference of the machine conditions so that it can attain a higher result.

Fig. 12 Classification results of SFAM

Additionally, in order to emphasize the improvement of the proposed framework where FB expansion is used as a pre-processing tool, SVM using one-against-all strategy is also implemented as a classifier to compare the performance with SFAM and the previous studies (Niu et al., 2008; Widodo et al., 2009). The kernel parameter γ and the regularization *C* in SVM are similarly chosen. The classification results are presented in Table 5. As observed, the training accuracy obtained from this study is similar to the previous works and achieves the highest value (100%). However, in the testing process, the proposed framework with SVM classifier provides a significantly higher result in comparison with those of the previous studies. Consequently, the proposed framework using FB expansion for signal preprocessing has considerably improved the accuracy of classification. Meanwhile, SVM classifier has a lower accuracy (98.57%) in comparison with SFAM (100%) due to the overlaps mentioned in previous section. This indicates that SFAM is a worth classifier which is not only fast in learning but also accurate in diagnosing.

Table 5 The comparison of classification results using SVM

3.5. Comparison with the use of HVD to the framework

In this section, a comparative study of using FB and HVD decompositions to the framework is carried out. According to the characteristics of HVD, the component signals decomposed from the original is gradually reduced amplitude, i. e. the first component contains the highest amplitude and the residual signal contains information of other lower amplitude components.

Hence, the similarity could occur in the first decomposed components of all machine conditions. For instance, as shown in Fig. 13 which depicts the results of HVD decomposition process of BR and ECC, the first components are very indistinguishable whilst the second and the third are easy to recognize the differences. Accordingly, the second and the third components are selected for fault diagnosis. The process of the feature extraction, feature reduction, and training classifier are similarly carried out. The accuracy of all values of VP in training mode achieves 100% while the testing results of classification are presented in Fig. 14. It can be seen that, the accuracy of the component 3 is higher than that of the component 2 and reaches the maximum of 98.57% for the values of VP from 0.2 to 0.6. However, it is still lower than that of using FB to the framework. This indicates that FB is better than HVD in preprocessing signal for fault diagnosis of induction motor using transient signal.

Fig. 13 HVD decomposition of a) BR condition, b) ECC condition
Fig. 14 Classification results of using HVD to the proposed framework

4. Summary and conclusions

This paper has presented the novel data driven-based fault diagnosis framework for induction motors using the transient current signal. Its implementation follows three consecutive stages. Firstly, the transient current signals of motor conditions are decomposed into the single component signals using Fourier-Bessel expansion. As a result, four single components are separated from each phase of the original motor current. In the second stage, statistical features in the time domain and the frequency domain are extracted from each component. The generalized discriminant analysis (GDA) is then used as the feature manipulation tool to reduce the high dimensionality of the original features and increase the separation between the motor conditions. Finally, the SFAM classifier is applied to the extracted features to accurately identify the conditions of the motors.

The accuracy of the SFAM classifier achieves the highest result where is of 100% in training and testing. A comparative study of the performance of this framework where SVM has been used as a classifier and those of the previous studies has been carried out. The results show that the proposed framework not only eliminates the smoothing and subtracting process used in previous works but also significantly improves the classification accuracy. Furthermore, SFAM provides a better performance in comparison with SVM. Additionally, HVD has been introduced to the framework as a preprocessing tool in order that the effectiveness of FB and HVD is appraised. The results illustrates that the accuracy obtained from FB is higher than that of HVD. It is eminently suitable to use for real fault diagnosis applications.

References

Arfken, G. (1996). *Mathematical methods for physicists*. Accademic Press, New York and London.

Baudat, G., & Anouar, F. (2000). Generalized discriminant analysis using a kernel approach. *Neural Computation, 12*, 2385-2404.

Benbouzid, M., (2000). A review of induction motors signature analysis as a medium for faults detection. *IEEE Transactions on Industrial Electronics, 47*, 984-993.

Bonnett, A. H. (1992). Cause and analysis of stator and rotor failures in three-phase squirrel-cage induction motors. *IEEE Transactions on Industry Applications, 28*, 921-937.

Cabal-Yepez, E., Romero-Troncoso, R. J., Garcia-Perez, A., & Osornio-Rios, R. A. (2012). Single-parameter fault identification through information entropy analysis at the startup-transient current in induction motors. *Electric Power Systems Research, 89*, 64-69

Candel, S. M. (1981a). An algorithm for the Fourier-Bessel transform. *Computer Physics Communication, 23*, 343-353.

Candel, S. M. (1981b). Dual algorithms for fast calculation of the Fourier-Bessel transform. *IEEE Transaction on Acoustics, Speech and Signal Processing, 29*, 963-972

Carpenter, C. A., Grossberg, S., Markuzon, N., Reynolds, J. H., & Rosen, D. B. (1992). Fuzzy ARTMAP: a neural network architecture for incremental supervised learning of analog multidimensional maps. *IEEE Transaction of Neural Networks, 3*, 698-713

Cavanagh, E., & Cook, B. (1979). Numerical evaluation of Hankel transforms via Gaussian-Laguerre polynomial expansions. *IEEE Transaction on Acoustics, Speech and Signal Processing, 27*, 361-366

Chen, C. S., & Gurgen, F .S. (1990). Speech enhancement by Fourier-Bessel coefficients of speech and noise. *IEE Proceedings of Communications, Speech and Vision, 137*, 290-294

D'Elia, G., Delvecchio, S., & Dalpiaz, G. (2012). On the use of Fourier-Bessel series expansion for gear diagnostics. *Proceedings of the Second International Conference on Condition Monitoring of Machinery in Non-Stationnary Operations*, 267-275

Douglas, H., & Pillay, P. (2005). The impact of wavelet selection on transient motor current signature analysis. *Proceedings of IEEE International Conference on Electric Machines and Drives*, pp. 80-85

Ebrahimi, B. M. , Faiz, J., Lotfi-fard, S., & Pillay, P. (2012). Novel indices for broken rotor bars fault diagnosis in induction motors using wavelet transform. *Mechanical Systems and Signal Processing, 30*, 131-145

Elkasabgy, N., Eastham, A., & Dawson, G. (1992). Detection of broken bars in the cage rotor on an induction machine. *IEEE Transactions on Industry Applications, 28*, 165-171.

Feldman, M. (2006). Time-varying decomposition and analysis based on the Hilbert transform. *Journal of Sound and Vibration, 295*, 518-530

Feldman, M. (2008). Theoretical analysis and comparison of the Hilbert transform decomposition methods. *Mechanical Systems and Signal Processing, 22*, 509-519.

Feldman, M. (2011). *Hilbert transform applications in mechanical vibration*. John Wiley & Sons.

Gopalan, K. (2001). Speech coding using Fourier-Bessel expansion of speech signals. *Proceeding of the IEEE Annual Conference on Industrial Electronics Society, 3*, 2199-2203

Gopalan, K., Anderson, T. R., & Cupples, E. J. (1997). Speaker identification using features based on first order Bessel function expansion of speech. *IEEE Pacific Rim Conference on Communications, Computer and Signal Processing, 2*, 589-592.

Guizar-Sicairos, M., & Gutierrez-Vega, J.C. (2004). Computation of quasi-discrete Hankel transforms of integer order for propagating optical wave fields. *Journal of the Optical Society of America, A 21*, 53-58.

Henry, D., Zolghadri, A., Monsion, M., & Cazaurang, F. (2002). Fault diagnosis in induction machines using the generalized structured singular value. *Control Engineering Practice, 10*, 587-598.

Huang, N. E., Shen, Z., Long, S. R., Wu, M. C., Shih, H. H., Zheng, Q., Yen, N. C., Tung, C. C., & Liu, H. H. (1998). The empirical mode decomposition and Hilbert spectrum for nonlinear and nonstationary time series analysis. *Proceedings of the Royal Society, A 454*, 903-995.

Jervis, B. W., Garcia, T., & Giahnakis, E. P. (1999). Probabilistic simplified fuzzy ARTMAP (PSFAM). *IEE Proceeding on Science, Measurement and Technology, 146*, 165-169

Kasuba, T. (1993). Simplified fuzzy ARTMAP. *AI Expert, 8*, 19-25.

Kim, T. -K., & Kittler, J. (2005). Locally linear discriminant analysis for multimodally distributed classes for face recognition with a single model image. *IEEE Transactions on Pattern Analysis and Machine Intelligence, 27*, 318-327

Kliman, G. B., Koegl, R.A., Stein, J., Endicott, R.D., & Madden, M.W. (1988). Non-invasive detection of

broken bars in operating induction motors. *IEEE Transactions on Energy Conversion, 3*, 873-879.

Nandi, S., Bharadwaj, R., Toliyat, H. A., & Parlos, A.G. (1998). Performance analysis of a three phase induction motor under mixed eccentricity condition. *Proceedings of the International Conference on Power Electronic Drives and Energy Systems for Industrial Growth, 1*, 123-128.

Niu, G., Widodo, A., Son, J. -D., Yang, B. -S., Hwang, D. -H., & Kang, D. -S. (2008). Decision-level fusion based on wavelet decomposition for induction motor fault diagnosis using transient current signal. *Expert Systems with Applications, 35*, 918-928

Oppenheim, A. V., Frisk, G. V., & Martinez, D. R. (1978). An algorithm for the numerical evaluation of the Hankel transform. *Proceedings of the IEEE, 66*, 264-265

Oppenheim, A. V., Frisk, G. V., & Martinez, D. R. (1980). Computation of the Hankel transform using projections. *Journal of Acoustical Society of America, 68*, 523-529

Pachori, R. B., & Sircar, P. (2007). A new technique to reduce cross terms in the Wigner distribution. *Digital Signal Processing, 17*, 466-474

Pachori, R. B., & Sircar, P. (2008). EEG signal analysis using FB expansion and second-order linear TVAR process. *Signal Processing, 88*, 415-420

Palaniappan, R., & Eswaran, C. (2009). Using genetic algorithm to select the presentation order of training patterns that improves simplified fuzzy ARTMAP classification performance. *Applied Soft Computing, 9*, 100-106

Peng, Z. K., Tse, P. W., Chu, F. L. (2005). An improved Hilbert-Huang transform and its application in vibration signal analysis. *Journal of Sound and Vibration, 286*, 187-205

Qin, S. R., & Zhong, Y. M. (2006). A new envelope algorithm of Hilbert-Huang transform. *Mechanical Systems and Signal Processing, 20*, 1941-1952

Rajasekaran, S., & Pai, G. A. V. (2000a). Simplified fuzzy ARTMAP as pattern recognition. *Journal of Computing in Civil Engineering, 14*, 92-99

Rajasekaran, S., & Pai, G. A. V. (2000b). Image recognition using simplified fuzzy ARTMAP augmented with a moment based feature extractor. *International Journal of Pattern Recognition and Artificial Intelligence, 14*, 1081-1095.

Ramesh Babu, T., Srikanth, S., & Sekhar, A. S. (2008). Hilbert-Huang transform for detection and monitoring of crack in a transient rotor. *Mechanical Systems and Signal Processing, 22*, 905-914

Rato, R. T., Ortigueira, M. D., & Batista, A. G. (2008). On the HTT, its problems, and some solutions. *Mechanical Systems and Signal Processing, 22*, 1374-1394

Schoen, R. R., Habetler, T. G., Kamran, F., & Bartheld, R. G. (1995a). Motor bearing damage detection using stator current monitoring. *IEEE Transactions on Industry Applications, 36*, 1274-1279.

Schoen, R. R., Lin, B., Habetler, T., Schlagy, J., & Farag, S. (1995b). An unsupervised, on-line system for induction motor fault detection using stator current monitoring. *IEEE Transactions on Industry Applications, 31*, 1280-1286.

Schroeder, J. (1993). Signal processing via Fourier-Bessel series expansion. *Digital Signal Processing, 3*, 112-124

Thomson, W. T., & Fenger, M. (2001).Current signature analysis to detect induction motor faults. *IEEE Transactions on Industry Applications, 7*, 26-34.

Vuskovic, M., & Du, S. (2002). Classification of prehensile EMG patterns with simplified fuzzy ARTMAP networks. *Proceedings of the 2002 International Joint Conference on Neural Networks*, 2539-2544

Widodo, A., & Yang, B. -S. (2008). Wavelet support vector machine for induction machine fault diagnosis based on transient current signal. *Expert Systems with Applications, 35*, 307-316

Widodo, A., Yang, B. -S., Gu, D. -S., & Choi, B. -K. (2009). Intelligent fault diagnosis system of induction motor based on transient current signal. Mechatronics, 19, 680-689

Yang, B. -S., & Widodo, A. (2009). *Introduction of intelligent machine fault diagnosis and prognosis*. Nova Science Publishers Inc., New York.
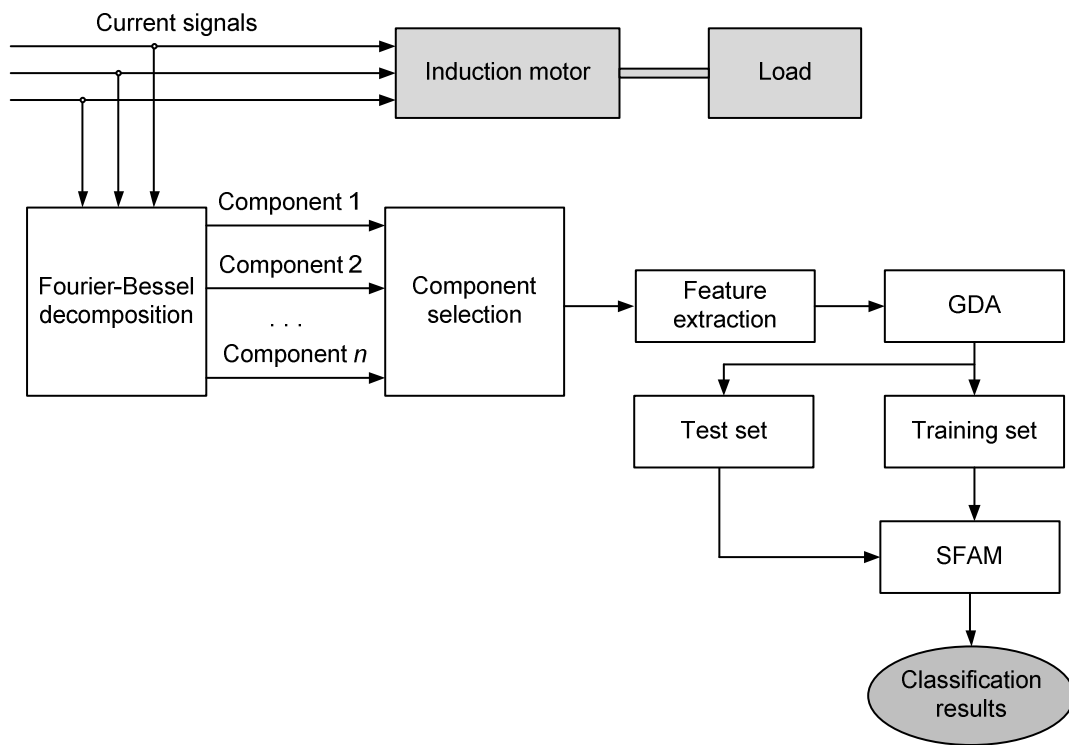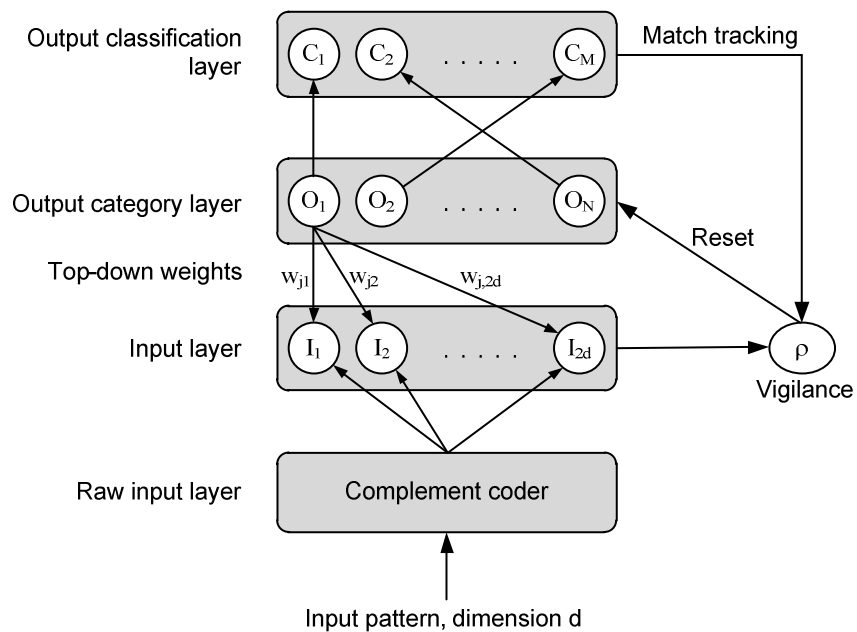
Fig. 1 The proposed framework for fault diagnosis

Fig. 2 The architecture of SFAM network
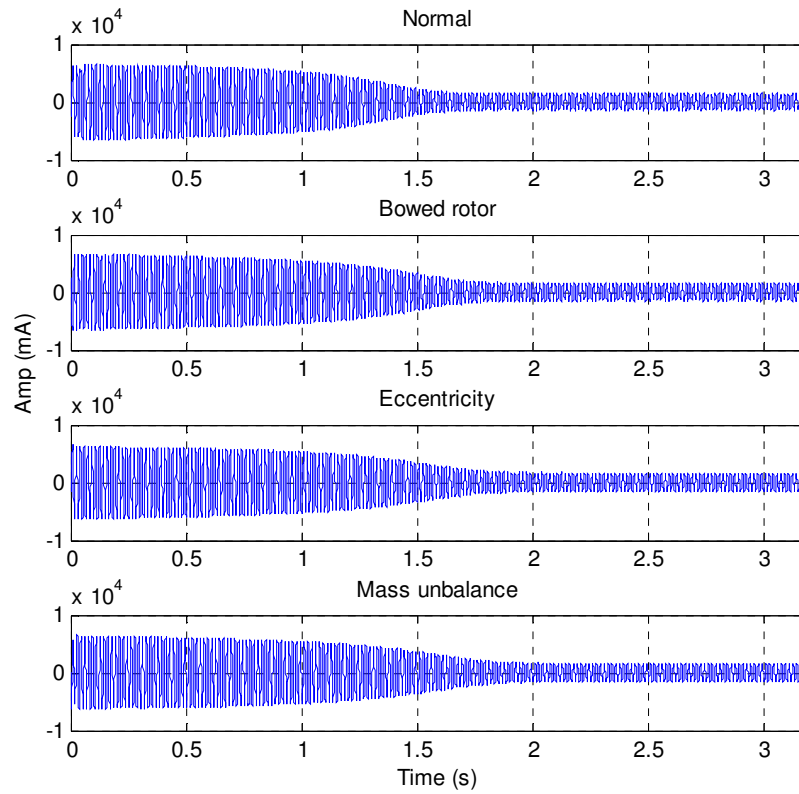
Fig. 3 Test rig for experiment

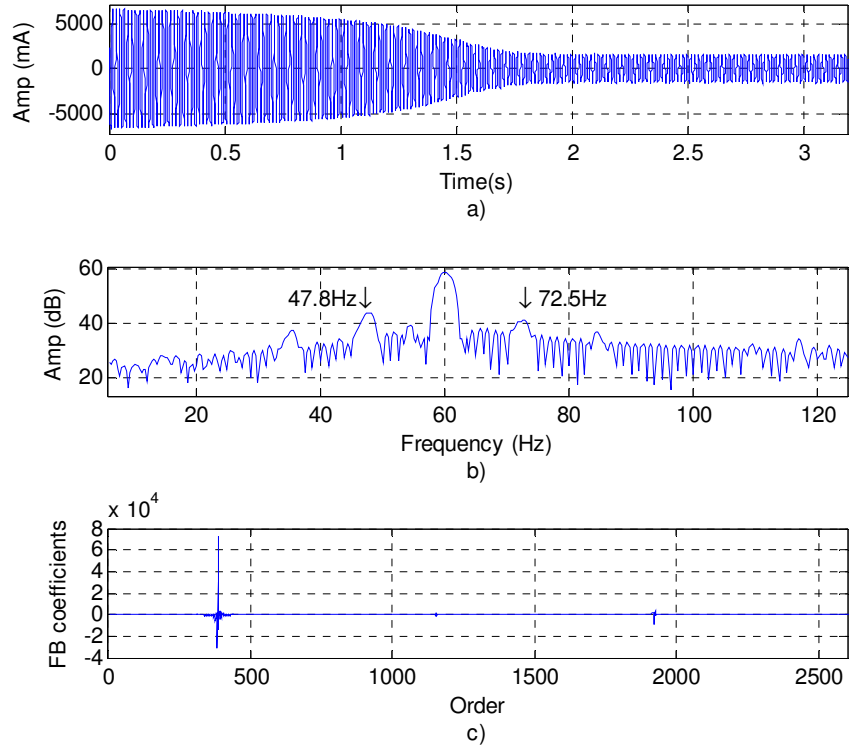**Fig. 4** The similarity of transient current signals

Fig. 5 a) Transient current signal of the bowed rotor in phase A, b) Current spectrum, c) FB coefficients
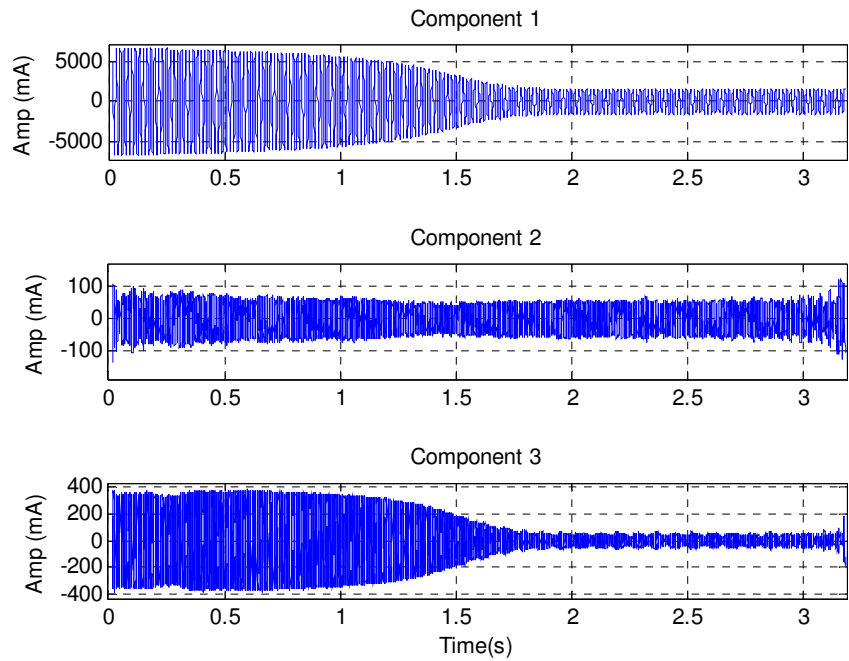

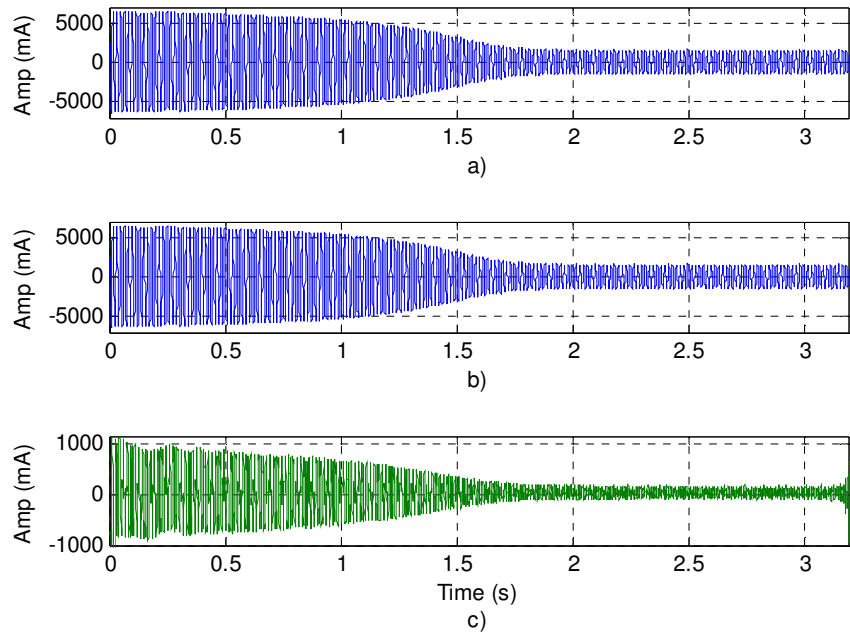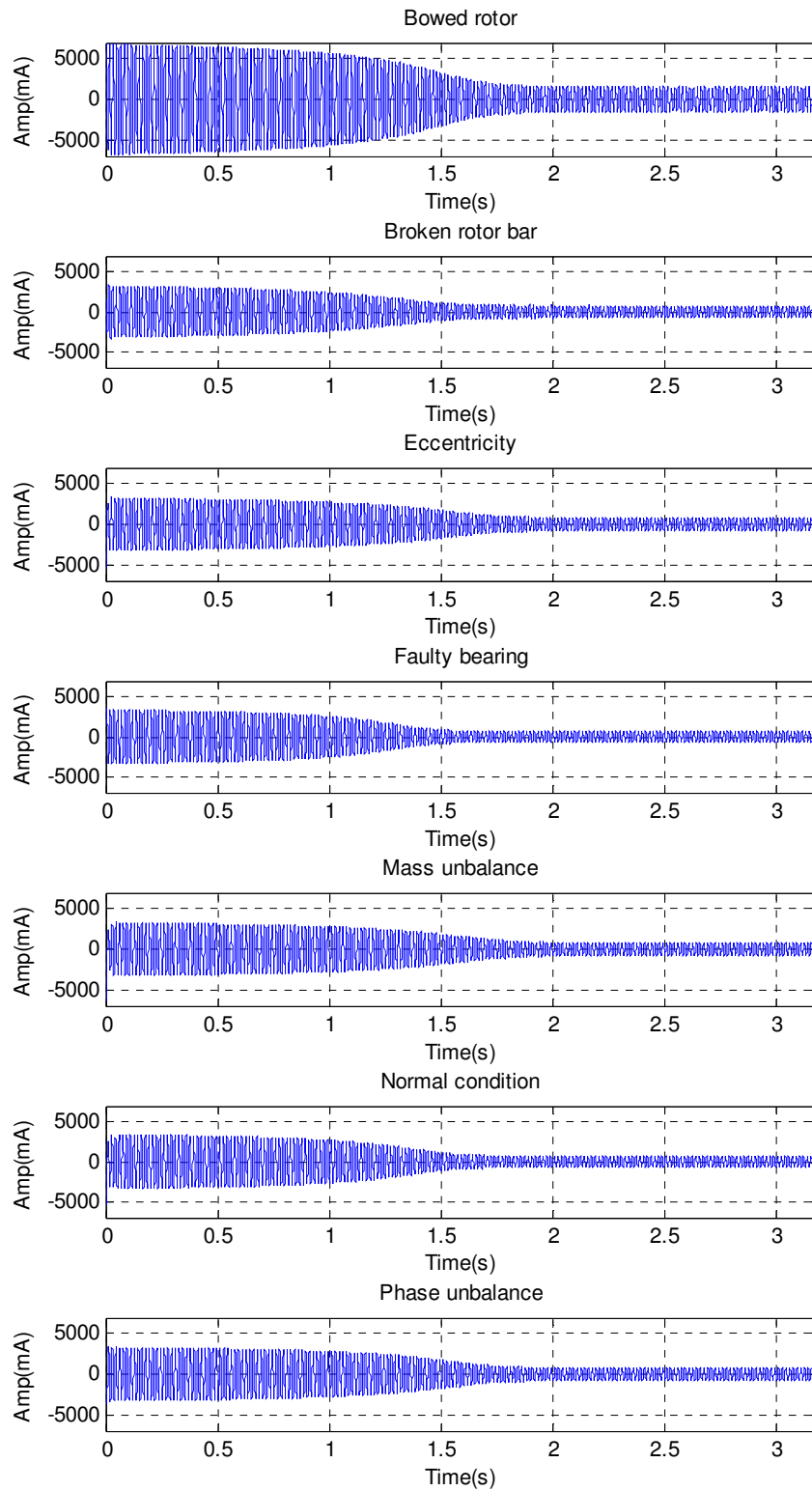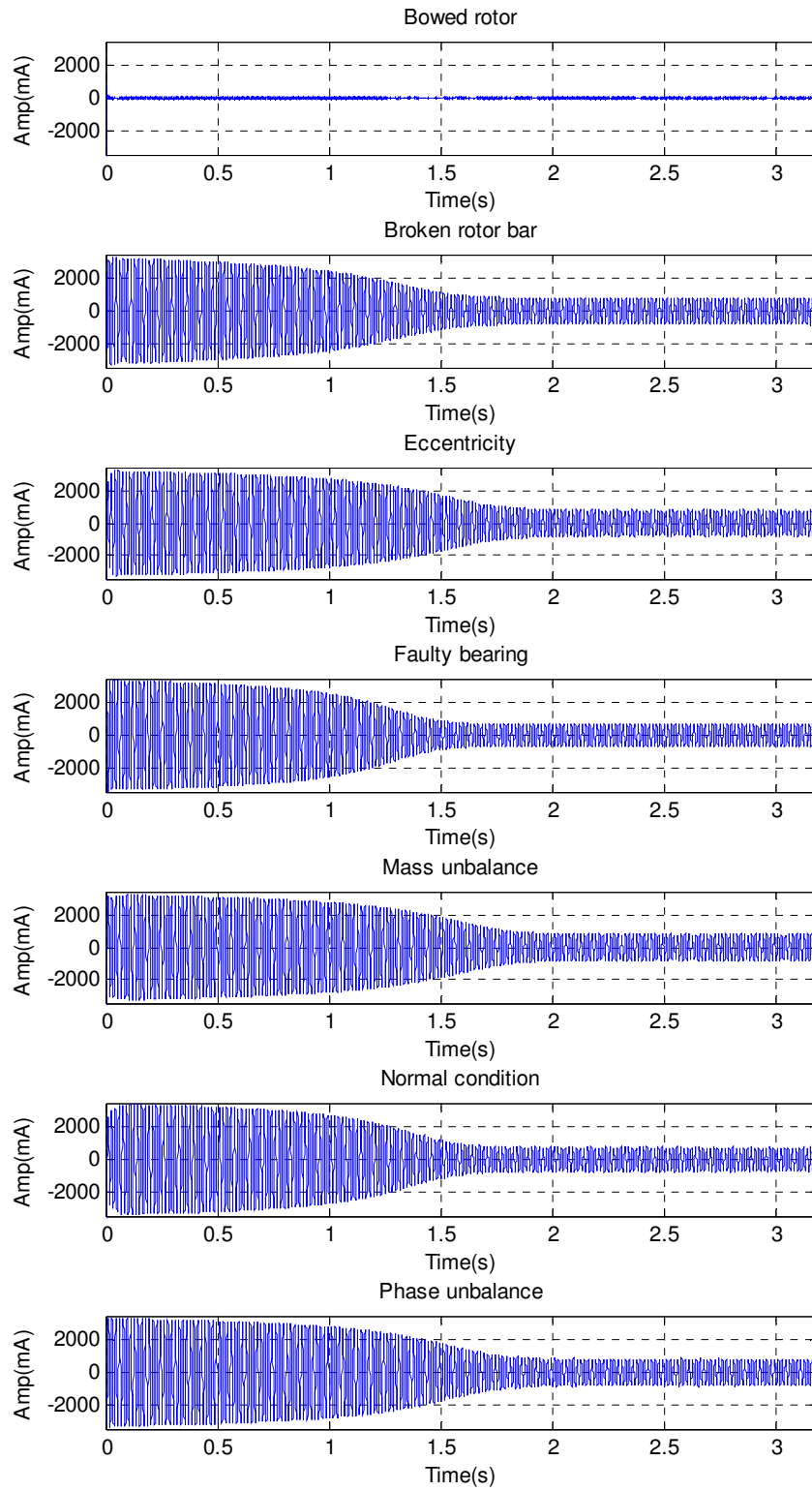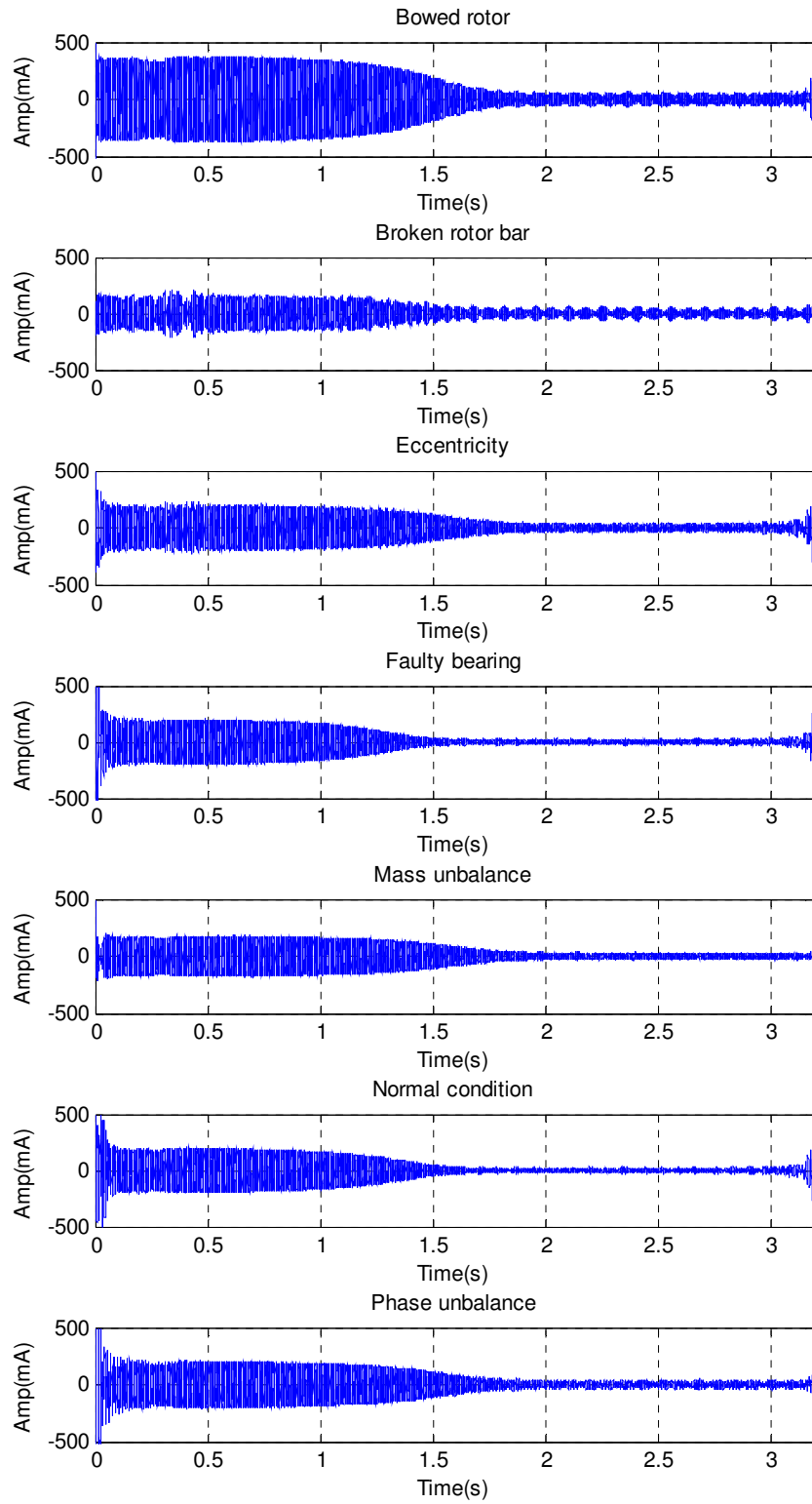**Fig. 6** Single components of the bowed rotor signal in phase A

Fig. 7 The bowed rotor signal in phase A: a) Original, b) Reconstructed, c) Residual

(a)

(b)

(c)
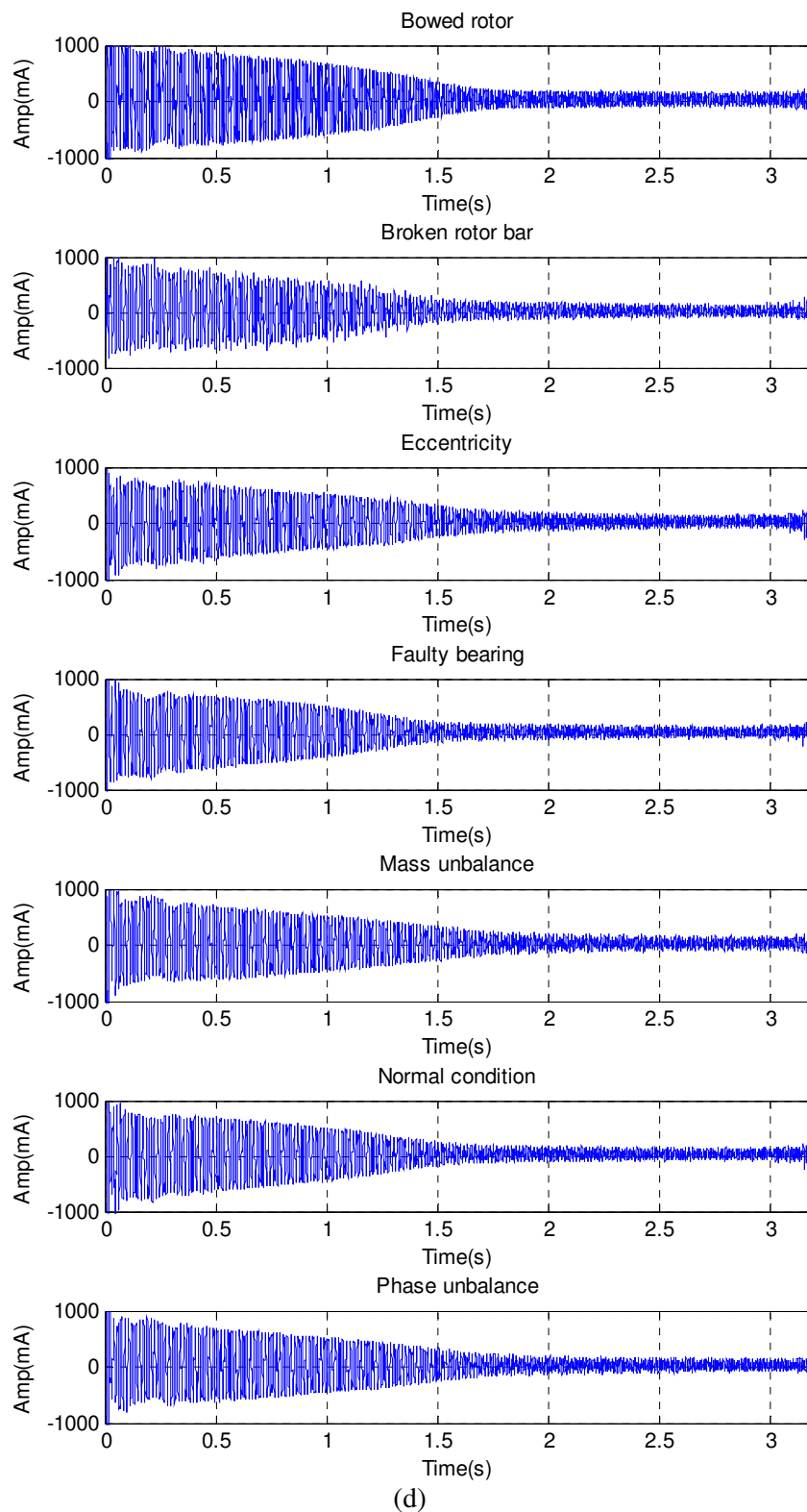
Fig. 8 The components of the motor conditions: a) Component 1, b) Component 2, and c) Component 3, and d) Component 4 (Residual)

24
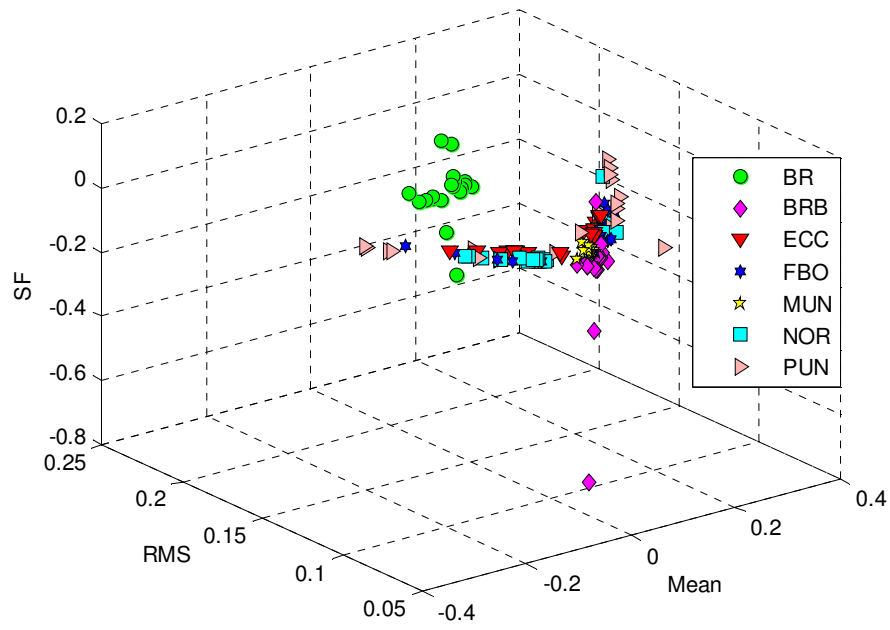
(a)
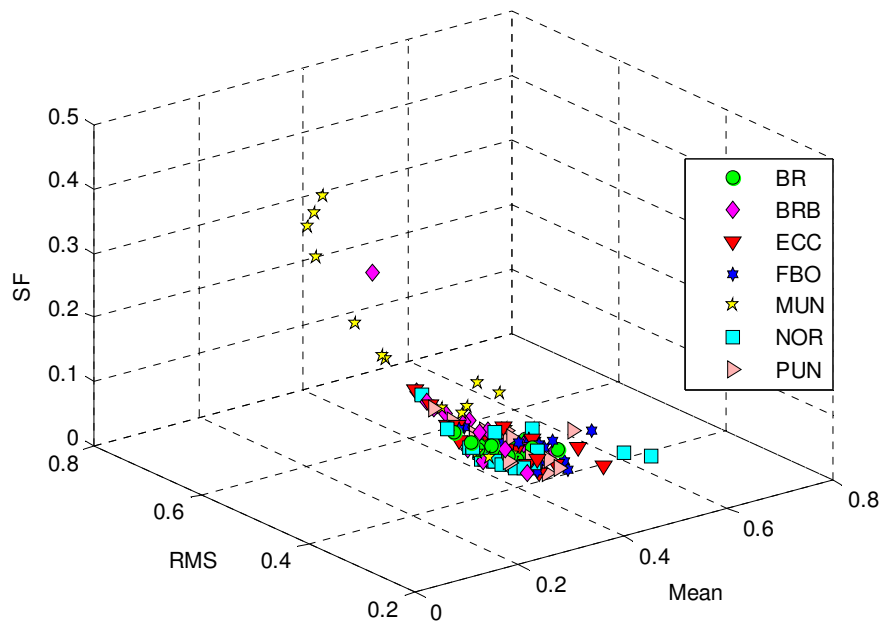
(b)

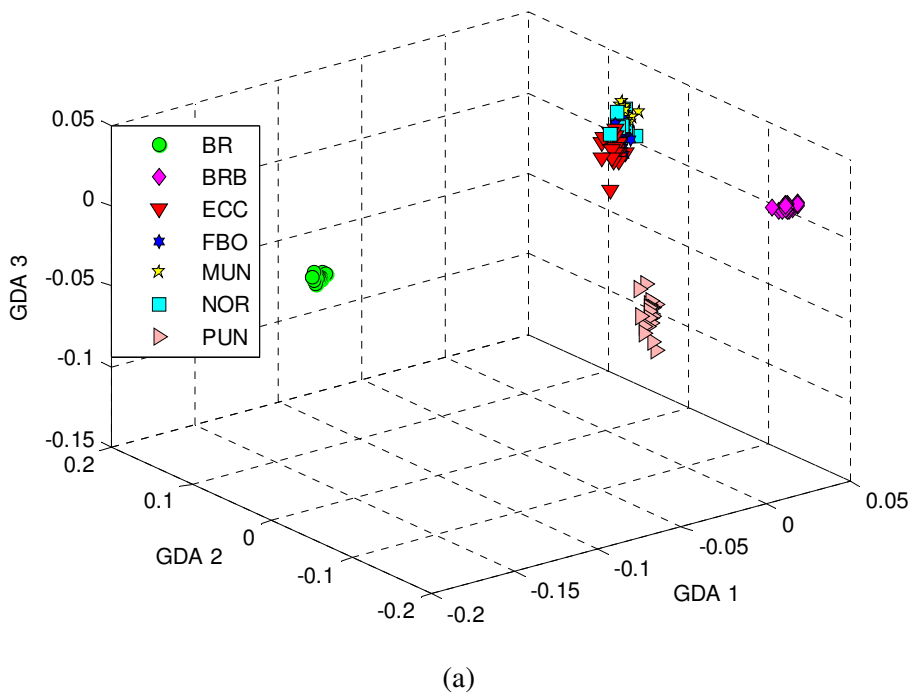**Fig. 9** The structure of the three-first features: a) Component 3, b) Component 4 (residual)
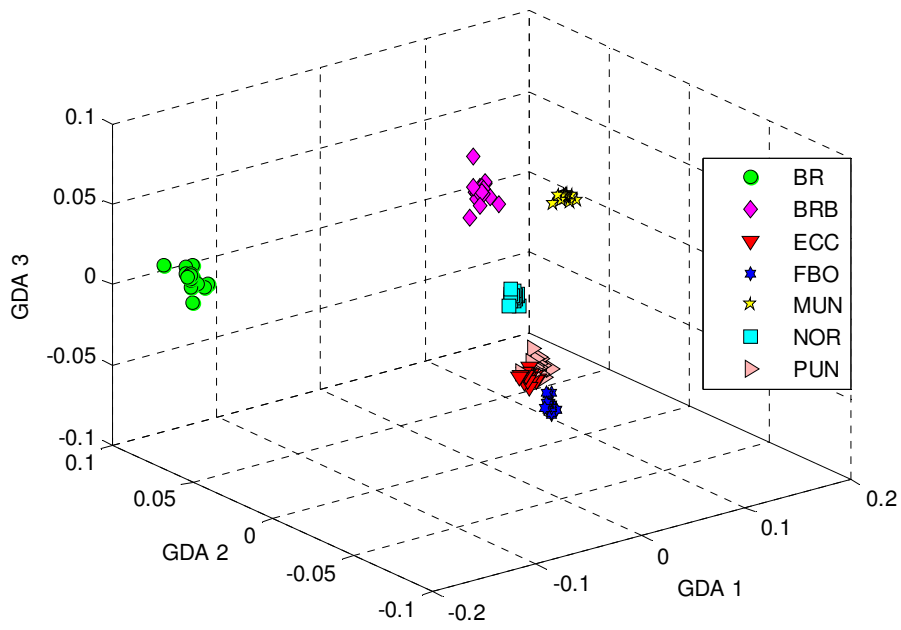
Fig. 10 Eigenvalue of covariance matrix for feature reduction

(a)
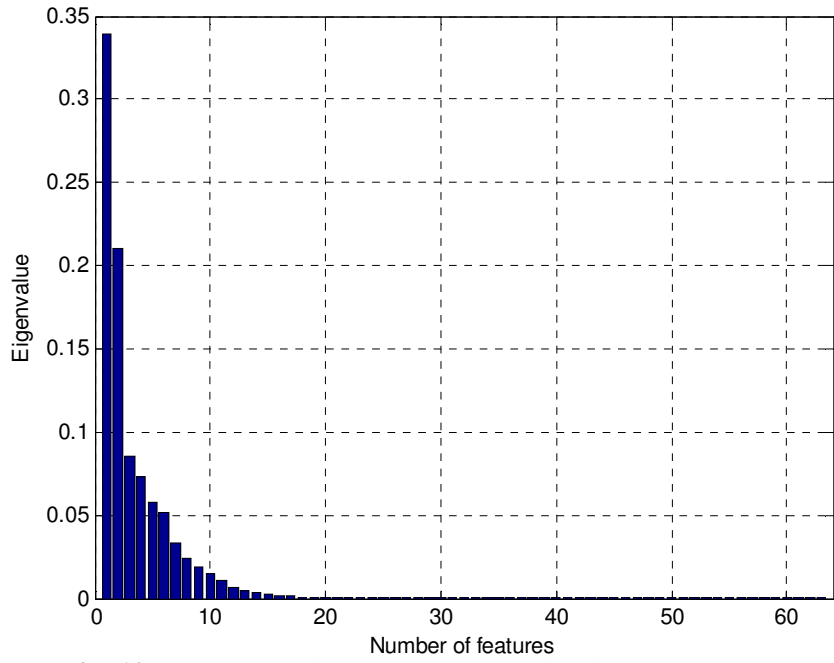
(b)

Fig. 11 The feature structure in the GDA space: a) Component 3, b) Component 4
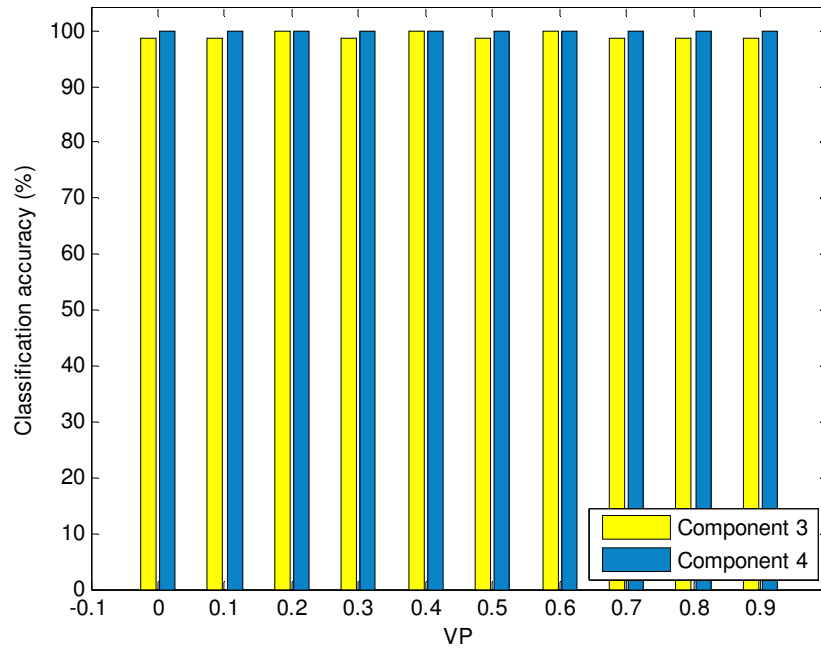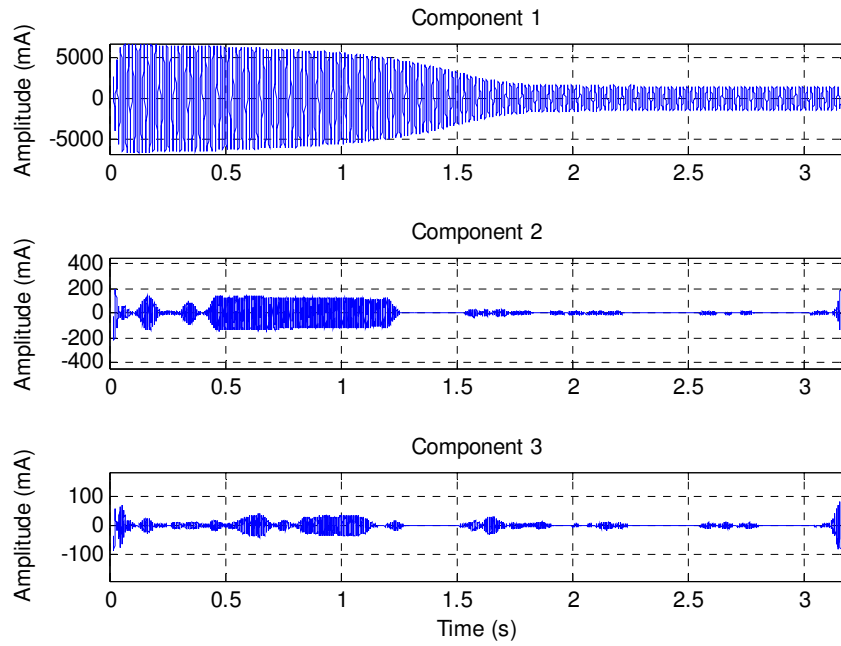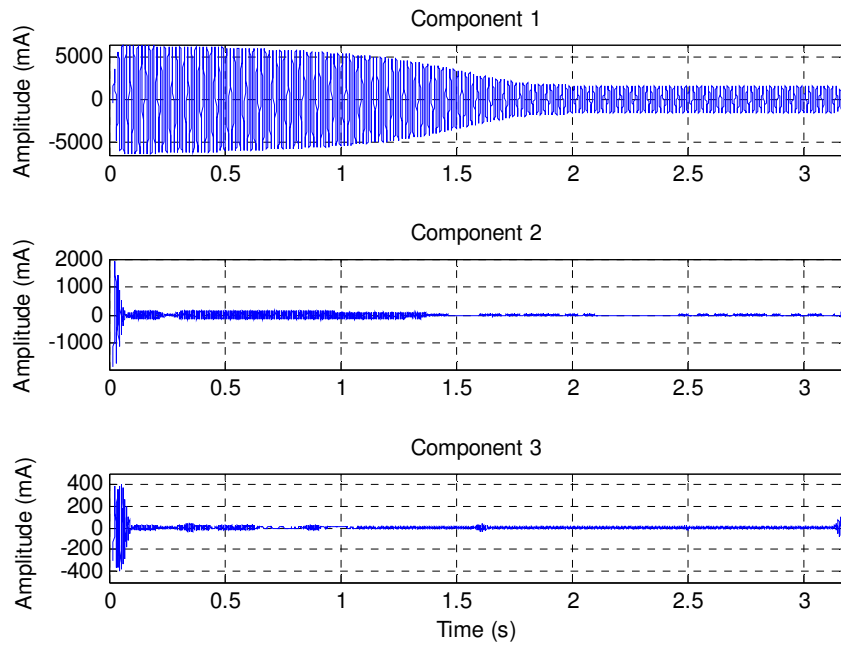

Fig. 12 Classification results of SFAM

Fig. 13 HVD decomposition of a) BR condition, b) ECC condition
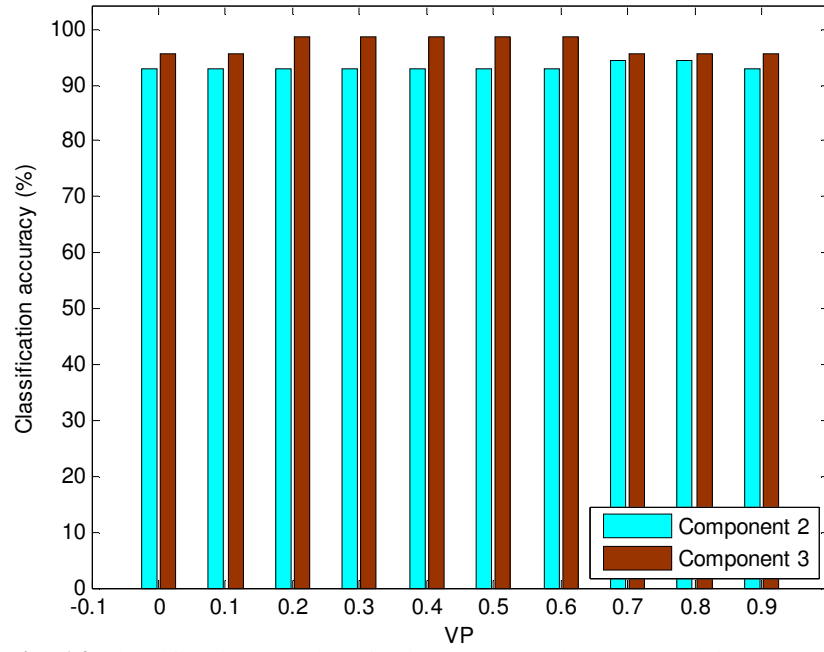
Fig. 14 Classification results of using HVD to the proposed framework

Table 1
The description of motor conditions

Fault condition	Fault description	Notes
Normal	Healthy condition	-
Bowed rotor	Maximum bowed shaft deflection: 0.075mm	Air-gap: 0.25mm
Broken rotor bar	Number of broken bars: 12	Total number of 34 bars
Eccentricity	Parallel and angular misalignments	Adjusting the bearing pedestal
Faulty bearing	spall on the outer raceway	#6203
Mass unbalance	Unbalance mass on the rotor	-
Phase unbalance	Add resistance on one phase	8.4%

Table 2
The statistical features in the time domain

Features	Expression	Notes
Mean	$m = \dfrac{1}{N}\sum_{i=1}^{N} x_i$	x_i is the ith value of signal x, N is the number of data points
RMS	$x_{rms} = \sqrt{\dfrac{1}{N}\sum_{i=1}^{N} x_i^2}$	
Shape factor	$SF = x_{rms} \Big/ \dfrac{1}{N}\sum_{i=1}^{N}\lvert x_i\rvert$	
Skewness	$Sk = \dfrac{1}{N}\sum_{i=1}^{N}(x_i - m)^3 \Big/ \left(\sqrt{\dfrac{1}{N}\sum_{i=1}^{N}(x_i - m)^2}\right)^3$	
Kurtosis	$Kur = \dfrac{1}{N}\sum_{i=1}^{N}(x_i - m)^4 \Big/ \left(\dfrac{1}{N}\sum_{i=1}^{N}(x_i - m)^2\right)^2$	
Crest factor	$CF = \max(x) \big/ x_{rms}$	
Entropy error	$E_e(x_i) = \sum p(x_i)\ln p(x_i)^2$	$p(x_i)$ is the distribution on the whole signal
Entropy estimation	$E_s(x_i) = -\sum p(x_i)\ln p(x_i)$	
Histogram lower	$h_L = \max(x_i) - \dfrac{\Delta}{2}$	$\Delta = \dfrac{\max(x_i) - \min(x_i)}{N-1}$
Histogram upper	$h_U = \max(x_i) + \dfrac{\Delta}{2}$	

Table 3

The statistical features in the frequency domain

Features	Expression	Notes
Frequency center	$FC = \sum_{i=2}^{N} \dot{x}_i x_i \Big/ 2\pi \sum_{i=1}^{N} x_i^2$	$\dot{x} = (x_i - x_{i-1})/\Delta$
RMS variance frequency	$RMSF = \sqrt{\sum_{i=2}^{N} \dot{x}_i^2 \Big/ 4\pi^2 \sum_{i=1}^{N} x_i^2}$	
Root variance frequency	$RVF = \sqrt{(\sum_{i=2}^{N} \dot{x}_i^2 \Big/ 4\pi^2 \sum_{i=1}^{N} x_i^2) - FC^2}$	

Table 4

The statistical features of regression estimation

Features	Expression	Notes
Auto-regression coefficients: a_1-a_8	$y_t = \sum_{i=1}^{n} a_i y_{t-i} + \varepsilon_t$	y_t is the signal under investigation, n is the order of auto-regression model, and ε_t is Gaussian white noise

Table 5

The comparison of classification results using SVM

	Classification accuracy (%)	
	Training	Testing
SVM applies for the component 4	100	98.57
SVM applied for the detail d2 (Niu et al., 2008)	100	90.0
SVM + PCA (Widodo et al., 2009)	100	76.19
SVM + ICA (Widodo et al., 2009)	100	83.33